BIOCHEMISTRY
including biophysical chemistry & molecular biology

Article

pubs.acs.org/biochemistry

Catalytic Characterization of Human Microsomal Glutathione *S*-Transferase 2: Identification of Rate-Limiting Steps

Shabbir Ahmad,[†] Damian Niegowski,[†] Anders Wetterholm,[†] Jesper Z. Haeggström,[†] Ralf Morgenstern,[‡] and Agnes Rinaldo-Matthis*[,†]

[†]Department of Medical Biochemistry and Biophysics, Chemistry II, Karolinska Institutet, Stockholm, Sweden

[‡]Institute of Environmental Medicine, Karolinska Institutet, Stockholm, Sweden

ABSTRACT: Microsomal glutathione *S*-transferase 2 (MGST2) is a 17 kDa trimeric integral membrane protein homologous to leukotriene C_4 synthase (LTC4S). MGST2 has been suggested to catalyze the biosynthesis of the pro-inflammatory mediator leukotriene C_4 (LTC_4) in cells devoid of LTC4S. A detailed biochemical study of MGST2 is critical for the understanding of its cellular function and potential role as an LTC_4-producing enzyme. Here we have characterized the substrate specificity and catalytic properties of purified MGST2 by steady-state and pre-steady-state kinetic experiments. In comparison with LTC4S, which has a catalytic efficiency of 8.7×10^5 M^{-1} s^{-1}, MGST2, with a catalytic efficiency of 1.8×10^4 M^{-1} s^{-1}, is considerably less efficient in producing LTC_4. However, the two enzymes display a similar $K_M^{LTA_4}$ of 30−40 μM. While LTC4S has one activated glutathione (GSH) (forming a thiolate) per enzyme monomer, the MGST2 trimer seems to display only third-of-the-sites reactivity for thiolate activation, which in part would explain its lower catalytic efficiency. Furthermore, MGST2 displays GSH-dependent peroxidase activity of ~0.2 μmol min^{-1} mg^{-1} toward several lipid hydroperoxides. MGST2, but not LTC4S, is efficient in catalyzing conjugation of the electrophilic substrate 1-chloro-2,4-dinitrobenzene (CDNB) and the lipid peroxidation product 4-hydroxy-2-nonenal with GSH. Using stopped-flow pre-steady-state kinetics, we have characterized the full catalytic reaction of MGST2 with CDNB and GSH as substrates, showing an initial rapid equilibrium binding of GSH followed by thiolate formation. Burst kinetics for the CDNB−GSH conjugation step was observed only at low GSH concentrations (thiolate anion formation becoming rate-limiting under these conditions). Product release is rapid and does not limit the overall reaction. Therefore, in general, the chemical conjugation step is rate-limiting for MGST2 at physiological GSH concentrations. MGST2 and LTC4S exhibit distinct catalytic and mechanistic properties, reflecting adaptation to broad and specific physiological functions, respectively.

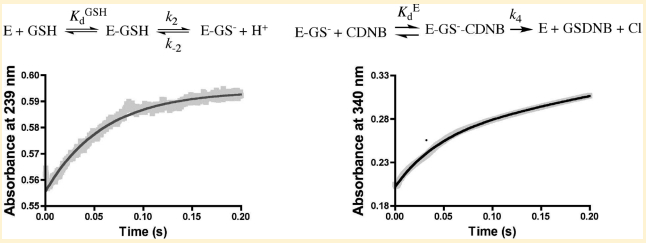

Microsomal glutathione *S*-transferase 2 (MGST2) belongs to the MAPEG (membrane-associated proteins in eicosanoid and glutathione metabolism) protein family. MAPEG proteins are involved in detoxification of xenobiotics as well as in the generation of pro-inflammatory compounds.[1] These proteins are integral trimeric membrane proteins, localized to the nuclear and endoplasmic reticulum membranes. MAPEG members have been found in mammals, plants, fungi, and bacteria.[2] The mammalian MAPEG members comprise six proteins, MGST1, MGST2, MGST3, LTC4S, five-lipoxygenase activating protein (FLAP), and microsomal prostaglandin E synthase (mPGES1), all related in sequence (20−40%) as well as in structure.[3] All but FLAP, for which no catalytic activity has been described, seem to share a similar catalytic mechanism, where binding and activation of GSH to form a thiolate is a common feature and a prerequisite for catalysis.

The family members have different functions, and the thiolate anion may be used to conjugate xenobiotic electrophiles for excretion, as for MGST1, as an oxidoreductant to convert prostaglandin $(PG)H_2$ into the pain- and fever-promoting PGE_2, as for mPGES-1, or as in LTC4S, to conjugate GSH with the epoxide LTA_4 producing the pro-inflammatory and spasmogenic mediator LTC_4. LTC_4 is the parent compound of the so-called cysteinyl-leukotrienes (cys-LTs) that include LTC_4, LTD_4, and LTE_4. These cys-LTs act as smooth muscle contracting agents through G-protein-coupled receptors, particularly in the respiratory tract, and are established and clinically significant mediators of asthma amenable for therapeutic intervention.[4]

LTC4S catalyzes the committed step in the formation of LTC_4 and is a potential drug target for the development of anti-asthma medications.[4] The published three-dimensional crystal structure of LTC4S[5] together with the recent characterization of the catalytic mechanism of LTC4S has provided important new insights into the molecular mechanism of LTC_4 biosynthesis.[6−8]

LTC4S displays a narrow expression profile with mRNA and protein only in cells of myeloid origin such as eosinophils, mast cells, monocytes, and platelets. However, conversion of LTA_4 into LTC_4 has been observed in other cells such as endothelial

Received: October 17, 2012
Revised: January 29, 2013
Published: February 14, 2013

dx.doi.org/10.1021/bi3014104 | *Biochemistry* 2013, 52, 1755−1764

cells, and in mice with a targeted deletion of LTC4S, synthesis of LTC_4 was not significantly impaired in the testis.[9] These observations suggest that LTC_4 might be produced by an additional enzyme(s).[10] MGST2, with an amino acid sequence 44% identical to that of LTC4S, is one likely candidate and has been shown to possess LTC_4 synthase activity.[11] The MGST2 mRNA has a wide tissue distribution, with high abundance in human liver and endothelial cells, and lower mRNA levels in lung cells.[10] Furthermore, Sjöström et al. showed that MGST2 and not LTC4S is responsible for LTC_4 production in human umbilical vein endothelial cells.[12]

On the basis of these observations, in an attempt to improve our understanding of the role of MGST2 in LTC_4 biosynthesis, we have investigated the functional properties of MGST2 with regard to substrate specificity and catalytic mechanism.

With a combination of steady-state and pre-steady-state stopped-flow kinetics, we have determined the rate-determining steps and approximated the number of active sites promoting stabilization of the GSH thiolate, and concomitant proton release. This work contributes to our understanding of the basic enzymology of the MAPEG superfamily and MGST2 as a potential drug target for inhibition of the production of the pro-inflammatory mediator LTC_4.

EXPERIMENTAL PROCEDURES

Chemicals. Bromocresol purple was from Fluka Chemie AG (Buchs, Switzerland). Dodecyl maltoside (DDM) was obtained from Anatrace. LTA_4 was produced by saponification of LTA_4 methyl ester (Cayman) with LiOH [6% (v/v)] in tetrahydrofuran for 48 h at 4 °C. Lipid hydroperoxides were obtained from Cayman. All other chemicals were obtained from the common sources.

Cloning, Protein Expression, and Purification. The human *MGST2* cDNA (IMAGE cDNA clone 5277851, Medical Research Council geneservice, Cambridge, United Kingdom) was subcloned into pPICZA (Invitrogen). The cDNA, supplemented with an N-terminal sequence encoding a His_6 tag, and the vector were amplified via polymerase chain reaction, and the products were cotransformed into $CaCl_2$-competent *Escherichia coli* (TOP10, Invitrogen), utilizing the endogenous recombinase activity of *E. coli* to recombine the fragments. The protein-coding part of the resulting plasmid was verified by DNA sequencing (SeqLab, Göttingen, Germany) and transformed into yeast *Pichia pastoris* competent cells using the Pichia EasyComp Transformation kit (Invitrogen).

The expression and solubilization of the protein were conducted as previously described for LTC4S.[6] To purify the protein, a Ni-Sepharose column was packed with 5 mL of Ni-Sepharose Fast Flow (GE Healthcare Biosciences) by gravity flow. The column with the sample loaded was washed with 3 column volumes of buffer A [25 mM Tris (pH 7.8), 0.5 M NaCl, 10% glycerol, 0.2% DDM, and 5 mM β-mercaptoethanol] followed by an equal volume of buffer A containing 10 and 40 mM imidazole. MGST2 was eluted with buffer A containing 200 mM imidazole. The purity of the protein was checked by sodium dodecyl sulfate−polyacrylamide gel electrophoresis (SDS−PAGE) using a Pharmacia PhastSystem (Figure 1). MGST2 was desalted on PD-10 columns (GE Healthcare Biosciences) and eluted in buffer B [25 mM Tris (pH 7.8), 100 mM NaCl, 0.03% DDM, and 5 mM β-mercaptoethanol] or buffer C [20 mM Tris (pH 7.2), 100 mM NaCl, 0.03% DDM, and 5 mM β-mercaptoethanol], and the protein was stored frozen at −20 °C. Buffer B was used to prepare the enzyme for steady-state kinetic analysis. For pre-steady-state kinetics, the freshly prepared enzyme in buffer C was used. The enzyme was always prepared without glutathione. LTC4S was prepared as described previously.[6]

Protein Concentration Determinations. The protein concentrations were determined spectrophotometrically at 280 nm using a molar extinction coefficient ε_{280} of 30035 M^{-1} cm^{-1} for MGST2 (M_w = 17 kDa) in addition to the Lowry[13] and/or Bradford method.[14]

Steady-State Kinetics. All enzymatic assays were performed at 25 °C. The enzyme activity was measured spectrophotometrically under steady-state conditions and calculated from the initial rates of the enzyme-catalyzed reaction. The enzyme concentration used was 0.5 μM, and the initial rates were measured over 1−2 min in 25 mM Tris (pH 7.8), 100 mM NaCl, and 0.05% DDM. The concentrations of GSH and the second substrates were varied independently in the range of 0.01−0.5 mM 1-chloro-2,4-dinitrobenzene (CDNB), 0.02−0.7 mM 4-chloro-3-nitrobenzacetophenone (CNAP), 0.02−0.5 mM 4-chloro-3-nitrobenzamide (CNBAM), 0.02−1 mM 4-chloro-3-nitrobenzaldehyde (CNBAL), 0.01−0.1 mM 4-hydroxynonenal (4-HNE), and 0.1−5 mM GSH. The enzyme-catalyzed conjugation was followed by the increase in absorbance at 340 nm for CDNB (ε_{340} = 9.6 mM^{-1} cm^{-1}), 297 nm for CNAP (ε_{297} = 11.9 mM^{-1} cm^{-1}), 370 nm for CNBAM (ε_{370} = 3.1 mM^{-1} cm^{-1}), 304 nm for CNBAL (ε_{383} = 10.1 mM^{-1} cm^{-1}), and 224 nm for 4-HNE (ε_{224} = 13.7 mM^{-1} cm^{-1}). All substrates but GSH were diluted in ethanol and added to a final concentration of 2.5%. All measurements were taken in triplicate, and experimental data were fit with the Michaelis−Menten equation using MMFIT and RFFIT in SIMFIT (http://www.simfit.man.ac.uk) to calculate the kinetic parameters k_{cat}, K_M, and k_{cat}/K_M.

The inhibition constant (K_i) for GSO_3^- for binding to MGST2 was determined using the CDNB assay described above, in which the reaction mixtures contained constant levels of CDNB (0.2 mM), a varying amount of GSH (0.5−1 mM), five different concentrations of GSO_3^- (0−500 μM), and 0.1 μg of enzyme in buffer A. An inhibition constant (K_i) of 1 μM was calculated using GraphPad Prism.

LTC_4 Synthase and Peroxidase Assay. Enzymatic conjugation of LTA_4 with GSH to form LTC_4 was assessed by high-performance liquid chromatography (HPLC), as described previously.[6] The reaction was performed in 100 μL of 25 mM Tris (pH 7.8) buffer containing 100 mM NaCl, 0.05% DDM, 5 mM GSH, and MGST2 (0.78 μM) or LTC4S (0.12 μM) at room temperature with LTA_4 (7.5−120 μM). The reaction was terminated after 15 s by addition of 200 μL of MeOH and 100 μL of water. The product was analyzed by HPLC with a UV detector at 280 nm. Enzyme-catalyzed reduction of lipid hydroperoxides was also determined by HPLC. The reaction was performed in 25 mM Tris (pH 7.8) buffer containing 100 mM NaCl and 0.05% DDM at room temperature with 2 mM GSH, MGST2 (0.29 μM) and lipid peroxides, 5-hydroperoxyeicosatetraenoic acid (5-HpETE), 15-hydroperoxyeicosatetraenoic acid (15-HpETE), 13-hydroperoxyoctadecatetraenoic acid (13-HpODE), and 13-hydroperoxyoctadecatrienoic acid (13-HpOTrE) in a final volume of 100 μL. After 2 min, the reaction was stopped by the addition of 200 μL of stop solution [2:1:0.003 (v/v) acetonitrile/water/acetic acid], and 17-hydroxydocosatetraenoic acid was used as the internal standard. The product was analyzed by HPLC with UV detection at 235 nm. Finally, experimental data were fit to

the Michaelis–Menten equation using MMFIT and RFFIT in SIMFIT (http://www.simfit.man.ac.uk) to calculate the kinetic parameters k_{cat}, K_M, and k_{cat}/K_M.

UV Difference Spectroscopy. UV difference spectra of the enzyme mixed with GSH were recorded on a Philips PU8720 spectrophotometer at room temperature between 200 and 400 nm to observe the formation of thiolate anion. Spectra were recorded in 1 cm cuvettes with MGST2 with or without 0.5 mM GSH in 100 mM Tris-HCl (pH 7.2) with 0.05% DDM. Difference spectra were obtained by subtracting the spectra of the enzyme in buffer without GSH and in buffer with 0.5 mM GSH from that of the enzyme with 0.5 mM GSH. The formation of a thiolate anion was measured as an increase in absorbance at 239 nm. Upon inclusion of the strong inhibitor GSO_3^- (20 μM), no thiolate anion peak was observed as expected.

Stopped-Flow Experiments. An Applied Photophysics SX20 stopped-flow instrument equipped with one monochromator was used for all experiments; 55 μL from each of two syringes was rapidly mixed in the 10 mm path length cell if not otherwise indicated, and the signal was recorded. In general, three to six trace averages were used to fit theoretical expressions describing single exponentials. All experiments measuring pre-steady-state kinetics were performed at pH 7.2 and 20 °C, and the concentrations given below are the resulting final concentrations in the observation cell.

pK_a Determination. To determine the pK_a of the enzyme–GSH thiolate, we measured thiolate anion formation using the stopped-flow method at varying pH values. The enzyme (20 μM) in buffer C was rapidly mixed with 100 mM phosphate buffer (pH 5.5–7.0) or 100 mM Tris buffer (pH 7.0–7.9). The buffers also contained 0.03% DDM, 100 mM NaCl, 5 mM β-mercaptoethanol, and 0.5 mM GSH. We tested both buffers with 0.5 mM GSH at pH 7.1 to ensure that the choice of buffer did not influence GSH binding. At least three measurements were recorded at each pH, and the amplitude at 239 nm, corresponding to the amount of thiolate formed ($\varepsilon_{\text{thiolate anion}}$ = 5000 M^{-1} cm^{-1}), was plotted versus pH. The K_a (hence pK_a) was determined by fitting the data to the equation amplitude = max amplitude/(1 + $10^{-pH}/K_a$) in GraphPad Prism.

GSH Binding and Thiolate Anion Formation. Freshly purified MGST2 (20 μM) in buffer C was rapidly mixed with the same buffer containing 0.5–50 mM GSH. The increase in absorbance at 239 nm was followed and fit to a single-exponential equation. An optical path length of 10 mm was used except with 25–50 mM GSH, for which a 2 mm cell was employed to reduce the high background absorbance of GSH.

Proton Release. We calculated the rate of proton release using a stopped-flow experiment in which the enzyme (20 μM) in buffer B (pH 7.0) was rapidly mixed with buffer B containing 2 mM GSH (pH 7.0). The change in pH was followed as an absorbance decrease using the pH sensitive dye bromocresol purple at 588 nm. The decrease in absorbance at 588 nm was followed and fit to a single-exponential function.

GS^- Release. The rate of the release of GSH from the enzyme–GSH complex was measured upon rapid dilution of a mixture of MGST2 (20 μM) equilibrated with a nonsaturating amount of GSH (15 μM) in an equal volume of buffer C. The release of GSH (strictly speaking, GSH thiolate reprotonation) was followed by the loss of absorbance at 239 nm. GSH release was also followed at 239 nm in a different experiment in which 15 μM enzyme containing 1 mM GSH mixed with 5 mM GSO_3^- in the same buffer C and the loss of absorbance observed at 239 nm. The rate constant was obtained by fitting a single exponential with averaged (three traces) progression curve using GraphPad Prism or Pro-Data SX provided with the stopped-flow apparatus.

Determination of $K_d^{GS^-}$. The dissociation constant of the thiolate anion was obtained using GS^- formation experiments in which the formation of thiolate anion was followed at 239 nm by mixing 20 μM purified enzyme in buffer C with 25–1000 μM GSH in the same buffer. The amount of bound GSH calculated from the amplitude of the thiolate signal using an $\varepsilon_{\text{thiolate anion}}$ of 5000 M^{-1} cm^{-1} (y-axes for bound GSH) at each concentration of GSH (x-axes for free GSH) was recorded and plotted using Prism, where $K_d^{GS^-}$ was calculated.

Pre-Steady-State Kinetics of the Chemical Step. Enzyme (20 μM) in buffer C containing 0.5 mM GSH was rapidly mixed with CDNB (0.05–0.8 mM) or CNAP (0.2 mM) in the same buffer. The burst of product formation was recorded at 340 nm for CDNB. No burst was observed for CNAP where only the steady-state rate could be recorded (Figure 4B). The burst for CDNB was fit to a single exponential followed by the steady-state equation $A = A_0(1 - e^{-kt}) + mt$ + offset, where A is the calculated amplitude, A_0 is the amplitude of the exponential phase, t is the time, k is the rate constant, m is the slope of the reaction (steady-state rate), and the offset is the initial value of the data.

Product Release. Product (GSDNB) release was observed as a concomitant change in the intrinsic tryptophan fluorescence of the enzyme while MGST2 (20 μM), mixed with GSDNB (50 μM) in buffer C, was rapidly diluted in the same buffer. Measurements were performed in a stopped-flow spectrophotometer with an excitation wavelength of 280 nm and detected by fluorescent light collected through a 320 nm cutoff filter.

Kinetic Data Analysis. Nonlinear regression analysis was performed using GraphPad Prism (GraphPad Software Inc.) and SIMFIT. The stopped-flow data were analyzed using Pro-Data SX provided with the instrument.

RESULTS

Improved Enzyme Expression System. MGST2 has been shown to catalyze conversion of LTA_4 into the pro-inflammatory mediator LTC_4 in cells with a low level of expression of LTC4S.[10] Previous studies revealed that MGST2 from membrane fractions of microsomes from Sf9 cells expressing MGST2 produces LTC_4 with an efficiency similar to that of cells expressing LTC4S.[11] In this study, we have, for the first time, overexpressed and purified the recombinant human membrane protein MGST2 using *P. pastoris* (Figure 1). The expressed and purified protein was subject to steady-state and pre-steady-state kinetics to analyze the substrate specificity and catalytic mechanism.

Substrate Specificity. A main aim of this study was to assess the catalytic properties of purified MGST2 and compare them with those of LTC4S. Specific activities and steady-state kinetic constants for MGST2 and LTC4S are listed in Tables 1–4. For the GSH conjugating activity with LTA_4, MGST2 and LTC4S displayed catalytic efficiencies, $k_{cat}/K_M^{LTA_4}$, of 1.8×10^4 and 8.7×10^5 M^{-1} s^{-1}, respectively. Thus, MGST2 is ~48 times less efficient in converting LTA_4 into LTC_4 than LTC4S. The $K_M^{LTA_4}$ was similar for both enzymes, 40 and 30 μM, respectively. The catalytic constants of GSH, k_{cat}/K_M^{GSH} and K_M^{GSH}, for MGST2 and LTC4S were determined using CDNB

dx.doi.org/10.1021/bi3014104 | *Biochemistry* 2013, 52, 1755–1764

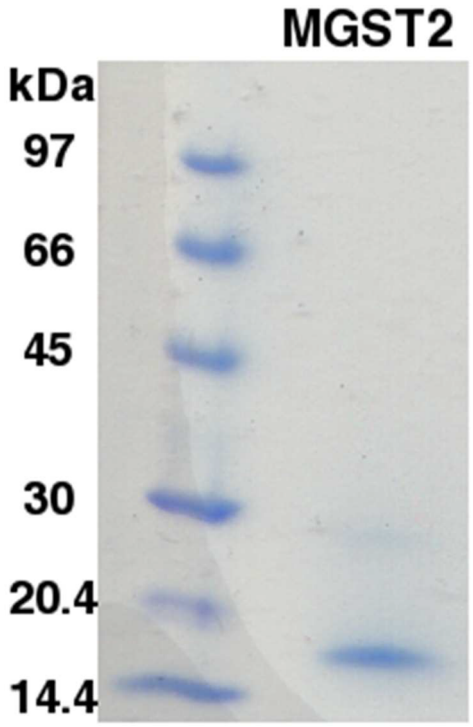

Figure 1. SDS−PAGE of purified human microsomal glutathione *S*-transferase 2: lane 1, molecular mass markers; lane 2, monomer band for purified microsomal glutathione *S*-transferase 2.

Table 1. Substrate Specificities of MGST2

substrate	specific activity (μmol min^{-1} mg^{-1})
epoxides	
LTA_4	1.23 ± 0.14
EPNP	<1.25
lipid hydroperoxides	
5-HpETE	0.25 ± 0.00
15-HpETE	0.21 ± 0.00
13-HpODE	0.20 ± 0.00
13-HpOTrE	0.16 ± 0.00
product from lipid peroxidation	
4-HNE	0.91 ± 0.10
electrophilic substrates	
CDNB	37.50 ± 1.50
CNBAL	2.55 ± 0.17
CNAP	0.43 ± 0.05
CNBAM	0.15 ± 0.02

Table 2. LTC_4 Production by Human LTC4S, MGST2, Cytosolic GST, and MGST1 with GSH and LTA_4 as Substrates[a]

enzyme	relative LTC_4 production (%)
LTC4S[7]	100
MGST2	3.4
cytosolic GST[27]	0.01
MGST1[25]	0.0006

[a] LTC_4 production was analyzed using HPLC with a UV detector at 280 nm as described in ref 6; 100% activity corresponds to 35 μmol of LTC_4 min^{-1} mg^{-1} produced by human LTC4S.

and LTA_4 as the second substrate, respectively. The catalytic parameters for GSH did not differ considerably; k_{cat}/K_M^{GSH} was 1.3×10^4 and 4×10^4 M^{-1} s^{-1} and K_M^{GSH} 1 and 0.3 mM for MGST2 and LTC4S, respectively (Table 3). For the glutathione-dependent peroxidase activity with lipid hydroperoxides (5-HpETE, 15-HpETE, 13-HpODE, and 13-HpOTrE), the catalytic efficiency of MGST2 ranged from 0.6×10^4 to 1.8×10^4 M^{-1} s^{-1}. The K_M values were in the low micromolar range (Table 3).

Among the major products generated endogenously from degradation of polyunsaturated fatty acids during lipid peroxidation (LPO) is 4-HNE. MGST2 was found to conjugate 4-HNE with GSH (0.9 μmol min^{-1} mg^{-1}), however with an efficiency lower than those with certain soluble GSTs, e.g., 1000 times lower than that of GSTA4-4, 10 times lower than that of GST A1-1,[15] and similar to that of MGST1.[16]

To test the catalytic efficiency of MGST2 with regard to the reactivity of the second substrate, we did a Hammett analysis. In this study, the Hammett analysis is used to study whether the chemical step is rate-limiting in the enzymatic reaction and not, as is most often the case, used to study the properties of the enzymatic reaction mechanism. The Hammett analysis was conducted using a series of electron deficient aryl substrates with different substituents para to the leaving group, CDNB, CNBAL, CNAP, and CNBAM (Table 3 and Figure 2). LTC4S was also tested with these substrates and did not display any detectable activity. MGST2 was most efficient with CDNB as the substrate [k_{cat}/K_M^{CDNB} of $(7.2 \pm 0.4) \times 10^4$ M^{-1} s^{-1}] followed by CNBAL [$k_{cat}/K_M^{CNBAL} = (2.3 \pm 0.2) \times 10^3$ M^{-1} s^{-1}], CNAP [$k_{cat}/K_M^{CNAP} = (3.6 \pm 0.4) \times 10^2$ M^{-1} s^{-1}], and CNBAM [$k_{cat}/K_M^{CNBAM} = (0.9 \pm 0.1) \times 10^2$ M^{-1} s^{-1}] (Table 3). When the logarithm of the obtained rate constant was plotted against the Hammet substituent constant (σ^-), a linear relationship was observed (Figure 2). The nonenzymatic rate of glutathione conjugation with the substrates displayed a slope (ρ) of 2.8 (where the slope reflects the degree to which chemical reactivity accounts for the trend in the obtained rate constants). A similar slope, 2.9, was obtained for log k_{cat} (and even higher for log k_{cat}/K_M), suggesting that chemistry is contributing substantially, i.e., governing the turnover of MGST2 at both nonsaturating (to be expected) and saturating second substrate concentrations.

Thiolate Anion Formation. The ability to form a thiolate anion is an important aspect of glutathione transferase catalysis. It has been shown in previous studies that LTC4S is able to stabilize a GS^- thiolate,[6] and here we wanted to determine whether MGST2 is able to do the same. A UV difference spectrum from 210 to 300 nm was recorded at pH 7.2 as a first indicator to detect the presence of a GSH thiolate anion. An increase in absorbance at 239 nm was observed (Figure 3A), demonstrating that the enzyme can lower the pK_a of GSH, which is around 8−9 in solution.[17] This absorbance could not be observed in the presence of the inhibitor GSO_3^-, and therefore, we concluded that the absorbance increase at 239 nm is due to GS^- and not to other changes of the protein. The amplitude of the A_{239} signal suggested a GS^-:MGST2 subunit stoichiometry of 1:3, which would indicate that one of three active sites in the MGST2 trimer is catalytically competent. To determine the pK_a of the enzyme−GSH thiolate, we measured thiolate anion formation using stopped-flow measurements at pH values varying from 5.5 to 7.9. For each pH, three to five measurements were recorded and the amplitude at 239 nm, corresponding to the amount of thiolate formed ($\varepsilon_{thiolate\ anion}$ = 5000 M^{-1} cm^{-1}), was plotted versus pH (Figure 3B). A pK_a of 6.3 was determined by fitting the data to the equation

dx.doi.org/10.1021/bi3014104 | *Biochemistry* 2013, 52, 1755−1764

Table 3. Catalytic Parameters of MGST2 and LTC4S

	MGST2			LTC4S		
substrate	k_{cat} (s^{-1})	K_M (μM)	k_{cat}/K_M (M^{-1} s^{-1})	k_{cat} (s^{-1})	K_M (μM)	k_{cat}/K_M (M^{-1} s^{-1})
LTA_4	0.6 ± 0.04	40 ± 6	(1.8 ± 0.2) × 10^4	26 ± 4	30 ± 10	(8.7 ± 4) × 10^5 [b]
GSH[a]	13.4 ± 0.50	1030 ± 110	(1.3 ± 0.1) × 10^4	12 ± 0.7	300 ± 60	(4.0 ± 1.1) × 10^4 [c]
5-HpETE	0.10 ± 0.01	5.2 ± 1	(1.8 ± 0.2) × 10^4	–	–	–
15-HpETE	0.15 ± 0.02	20 ± 5	(6.3 ± 0.9) × 10^3	–	–	–
13-HpODE	0.09 ± 0.003	9 ± 1	(9.7 ± 0.9) × 10^3	–	–	–
13-HpOTre	0.06 ± 0.002	5 ± 1	(1.1 ± 0.1) × 10^4	–	–	–
CDNB	14.30 ± 0.54	200 ± 20	(7.2 ± 0.4) × 10^4	–	–	–
CNBAL	1.60 ± 0.16	750 ± 140	(2.3 ± 0.2) × 10^3	–	–	–
CNAP	0.30 ± 0.07	850 ± 300	(3.6 ± 0.4) × 10^2	–	–	–
CNBAM	0.17 ± 0.05	1810 ± 700	(0.9 ± 0.1) × 10^2	–	–	–

[a]The second substrate is CDNB for MGST2 and LTA_4 for LTC4S. [b]From ref 6. [c]From ref 7.

Table 4. Microscopic Rate and Equilibrium Constants for Thiolate Anion Formation in MGST2, MGST1, and LTC4S

enzyme	K_D^{GSH} (mM)	k_2 (s^{-1})	k_{-2} (s^{-1})[a]	k_{-2} (s^{-1})[b]	$K_D^{GS^-}$ (μM)
MGST2	4.3 ± 0.6	41.1 ± 1.2	4.9 ± 1.2	2.0 ± 0.05	136 ± 55
MGST1[c]	11.7 ± 3.1	13.2 ± 0.9	0.2 ± 0.4	0.016 ± 0.00	22 ± 5
LTC4S[d]	3.0 ± 0.6	200 ± 26	–	1.3 ± 0.006	14.3 ± 2.4

[a]k_{-2} determined from the intercept at *y*-axes of the k_2 determination. [b]k_{-2} determined by the GS^- release experiment; average value of three to five traces. [c]From ref 19. [d]From ref 7.

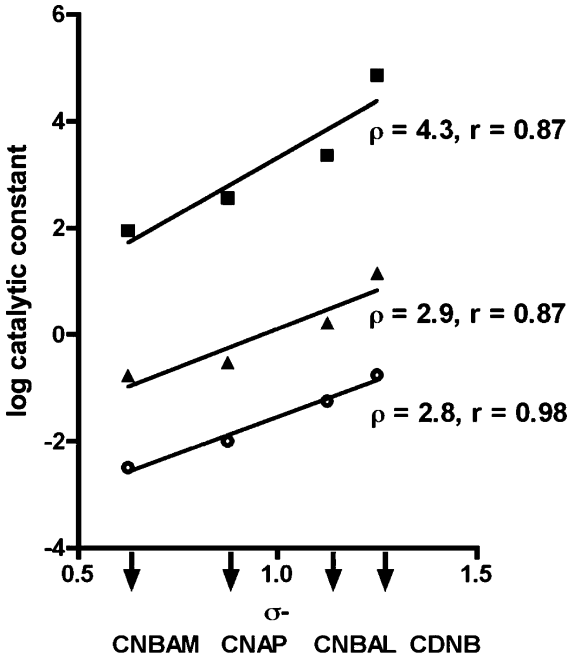

Figure 2. Hammett plot for the MGST2-catalyzed reaction of para-substituted 1-chloro-2-nitrobenzene derivatives with GSH at pH 7.8, as a function of the σ^- substituent constants. Nonenzymatic second-order rate constants (M^{-1} s^{-1}) are indicated by circles. Catalytic constants k_{cat} (s^{-1}) and k_{cat}/K_M (M^{-1} s^{-1}) are indicated by filled triangles and filled squares, respectively. Hammett ρ values and correlation coefficients (r) are indicated.

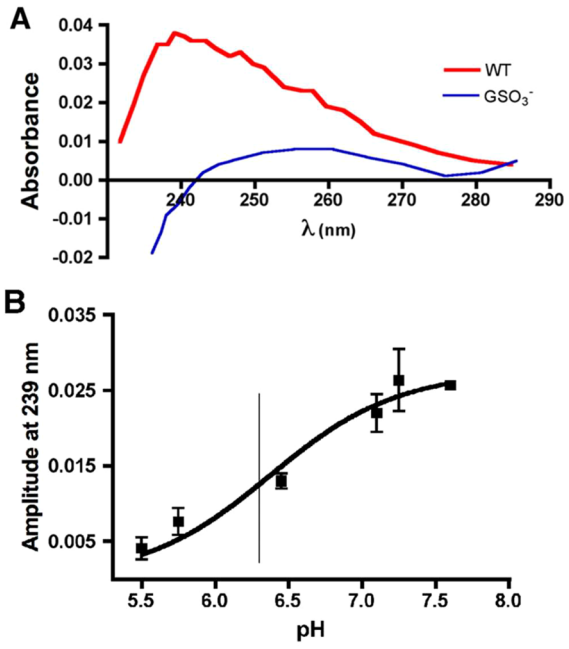

Figure 3. (A) UV difference spectra at pH 7.2, from 230 to 285 nm, show that a thiolate anion gives rise to a peak at 239 nm in the spectrum when MGST2 (20 μM) (red trace) is mixed with 0.5 mM GSH while no peak can be observed when MGST2 (20 μM) is incubated with 0.5 mM GSO_3^- (a competitive inhibitor) prior to GSH incubation (blue trace). (B) The pK_a of the thiol (GSH) bound to MGST2 was determined by following thiolate anion formation at 239 nm at different pH values by stopped-flow methods. A pK_a of 6.3, marked with a line, was determined by fitting the experimental data to the equation $Y = Y_{max}/(1 + 10^{-pH}/K_a)$, where Y is the amplitude at 239 nm and $K_a = (4.2 \pm 1) \times 10^{-7}$.

amplitude = max amplitude/$(1 + 10^{-pH}/K_a)$ in GraphPad Prism.

To study the rate behavior of thiolate anion formation, we used pre-steady-state stopped-flow analysis in which MGST2 was rapidly mixed with 0.5−50 mM GSH. The traces were fit with a single-exponential function to obtain the k_{obs} of thiolate anion formation, which exhibited saturable GSH concentration dependence (Figure 4B). The data were fit to a hyperbolic function (eq I) suggesting a two-step mechanism (eq II) with the rapid equilibrium formation of an initial complex (K_D^{GSH} = 4.3 ± 0.6 mM) followed by the appearance of the enzyme-bound thiolate (k_2 = 41 ± 1.2 s^{-1}). The k_{-2} obtained from the

dx.doi.org/10.1021/bi3014104 | *Biochemistry* 2013, 52, 1755−1764

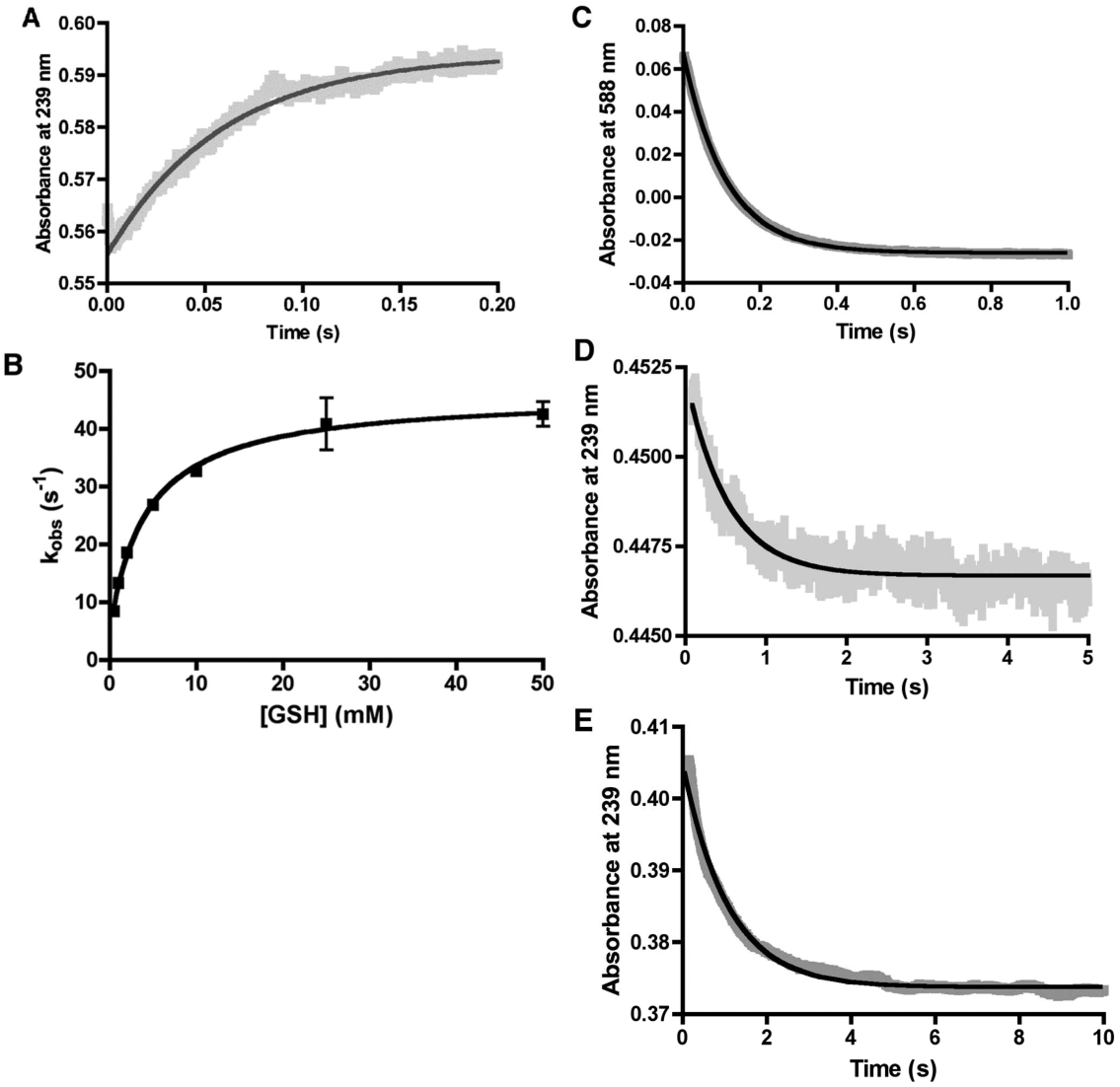

Figure 4. (A) Representative example of stopped-flow experimental traces (gray) of thiolate anion formation (A_{239}) when mixing 20 μM MGST2 with 2 mM GSH. The black line is a fit of the experimental trace to a single-exponential function with a k_{obs} of 18 s^{-1}. The observed amplitude corresponds to a stoichiometry of 0.33 per enzyme trimer. (B) Dependence of k_{obs} on the concentration of GSH where different k_{obs} rates from panel A were fit to eq I to obtain k_2, k_{-2}, and K_d^{GSH}. Two to five measurements were performed at each GSH concentration. (C) Proton release observed by the loss of absorbance at 588 nm (bromocresol purple) when MGST2 (20 μM) was mixed with GSH (2 mM). The traces are fit to single-exponential functions, which yields a rate of proton release, 9 s^{-1}, (D) Determination of the k_{-2} rate constant from a representative GSH release experiment. The absorbance at 239 nm was determined when a solution of 20 μM MGST2 and a nonsaturating amount of 15 μM GSH in buffer C were rapidly mixed with the same amount of a buffer C solution. A rate constant k_{-2} of 2.0 ± 0.05 s^{-1} was obtained by fitting the experimental data (gray) to a single-exponential function (black line) by averaging six traces. (E) Determination of k_{-2} from a GSO_3^- competition experiment in which the disappearance of GS^- was observed by the loss of absorbance at 239 nm. A fit to a single-exponential function gives a rate k_{-2} of 0.9 ± 0.01 s^{-1}.

y-intercept was 4.9 s^{-1}. To obtain a better estimate of k_{-2}, we performed an independent experiment measuring GSH release (see below).

Proton Release upon GSH Binding. When GSH is deprotonated to form a thiolate, the proton can be either taken up by a nearby residue on the protein or released to the solvent. Using bromocresol purple as a pH indicator, we measured the rate of proton release during GS^- formation at 588 nm using stopped-flow analysis. The proton release at 2 mM GSH was fit to a single-exponential function with a k_{obs} of 9 s^{-1} (Figure 4C). Although a double-exponential function fits the data somewhat better, the separation of the rate constants (12 and 6 s^{-1}) is small (not shown).

$$k_{obs} = k_{-2} + \frac{k_2[GSH]}{K_d^{GSH} + [GSH]} \quad \text{(I)}$$

$$E + GSH \overset{K_d^{GSH}}{\rightleftharpoons} E{-}GSH \underset{k_{-2}}{\overset{k_2}{\rightleftharpoons}} E{-}GS^- + H^+ \quad \text{(II)}$$

GSH Release Experiment. The rate of release of GSH from the enzyme−thiolate complex was studied using stopped-flow rapid dilution of a mixture of MGST2 in equilibrium with a nonsaturating amount of GSH.[7,18] The release of GSH was followed by the loss of absorbance at 239 nm. The data were fit to a single-exponential function showing a rate (Figure 4D), k_{-2}, of 2.0 ± 0.05 s^{-1}.

dx.doi.org/10.1021/bi3014104 | *Biochemistry* 2013, 52, 1755−1764

$K_d^{GS^-}$ Determination. To determine the affinity of MGST2 for deprotonated GSH ($K_d^{GS^-}$), we analyzed the amplitude of GS^- formed when the enzyme was rapidly mixed with GSH (25–1000 μM) (Figure 5). Bound GS^- plotted against the amount of free GSH was fit to the hyperbolic eq III, yielding a $K_d^{GS^-}$ of 136 ± 55 μM.

$$[\text{bound } GS^-] = \frac{B_{max}[\text{free GSH}]}{K_d^{GS-} + [\text{free GSH}]} \quad \text{(III)}$$

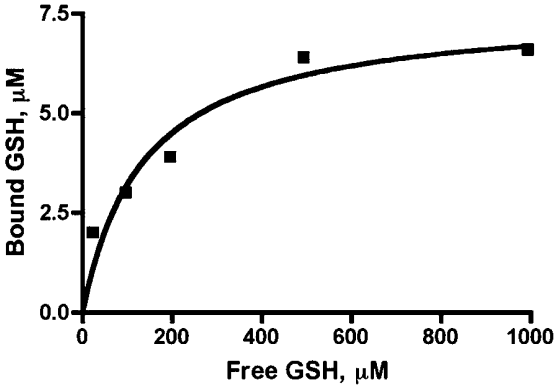

Figure 5. Determination of the dissociation constant of GS^- ($K_d^{GS^-}$) of MGST2. The enzyme (20 μM) was rapidly mixed with GSH (25–1000 μM), and the amount of GS^- (bound GSH) was calculated by converting the amplitudes at 239 nm to concentrations of thiolate using an $\varepsilon_{(thiolate)}$ of 5000 M^{-1} cm^{-1}. The $K_d^{GS^-}$ was obtained by plotting the amount of free GSH against the amount of bound GSH. The $K_d^{GS^-}$ of 136 ± 55 μM was calculated by fitting the experimental data to the hyperbolic eq III (see the text).

Kinetic Analysis of the Chemical Conjugation Step. To study the chemical step in catalysis (see scheme IV), pre-steady-state kinetic burst analysis was attempted with the two substrates, CDNB and CNAP. Rapid mixing using the stopped-flow method of the E–GS^- complex with CDNB resulted in a burst of product formation followed by a steady-state rate (Figure 6A) at low GSH concentrations. The burst kinetics suggests a rapid chemical step followed by a slower step, e.g., product release or recharging of thiolate. The traces were fit to a single-exponential equation followed by steady state. Plotting the concentration dependence of k_{obs} of the burst against the CDNB concentration, we observed a linear dependence without saturation behavior (Figure 6B). Therefore, the data were fit to eq V, simplified to $k_{obs} = k_4/K_D[\text{CDNB}]$ (where $K_D^E \gg [\text{CDNB}]$), which allows us to obtain the apparent second-order rate constant for the bimolecular reaction [k_4/K_D^{CDNB} = (9.9 ± 0.2) × 10^4 M^{-1} s^{-1}]. This value agrees well with the k_{cat}/K_M for CDNB as expected. Using lower concentrations of GSH in the experiment yielded an even more pronounced burst phase (not shown). This observation suggests that recharging of the enzyme with thiolate gradually becomes rate-determining as the GSH concentration is lowered and is not consistent with product release being a rate-limiting step.

CNAP did not display burst kinetics (Figure 6C), and the chemical step is therefore most probably rate-limiting for this reaction (at least there is no slower step after the chemical reaction has taken place).

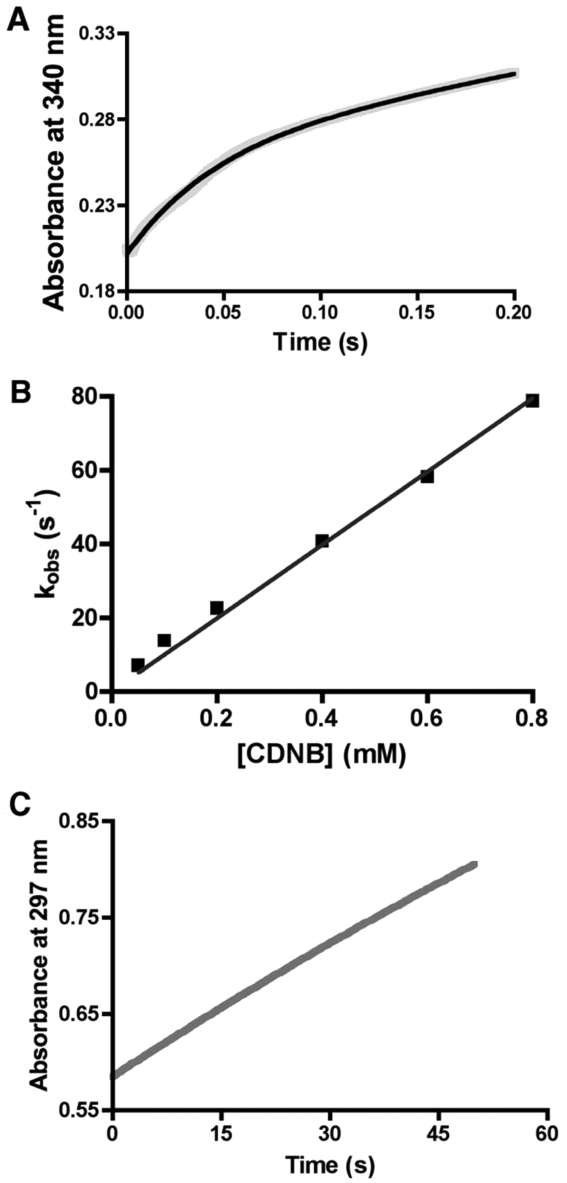

Figure 6. (A) Burst of product formation followed by steady state observed at 340 nm after rapid mixing of the E–GS^- complex (20 μM MGST2 and 0.5 mM GSH) with CDNB (0.2 mM). The black line is a fit of the experimental trace to a single exponential followed by steady state yielding a k_{obs} of the burst of 22 s^{-1} and a steady-state rate of 1 s^{-1}. The amplitude of the burst corresponds to 6.6 μM product. (B) The observed rates from the burst at varying CDNB concentrations were fit to a linear function (at low CDNB concentrations, $k_{obs} = k_4/K_D[\text{CDNB}]$), which yields only the apparent second-order rate constant k_4/K_D^E. (C) No burst of product formation and only the steady-state rate observed at 297 nm for the less reactive substrate CNAP (0.2 mM) mixed with the E–GS^- complex (20 μM MGST2 and 0.5 mM GSH).

$$E{-}GS^- + CDNB \overset{K_d^{CDNB}}{\rightleftharpoons} E{-}GS{-}CDNB \overset{k_4}{\rightarrow} E{-}GSDNB + Cl^- \quad \text{(IV)}$$

$$k_{obs} = \frac{k_4[\text{CDNB}]}{K_d^E + [\text{CDNB}]} \quad \text{(V)}$$

To confirm the suggestion that product release is not rate-limiting, we directly measured the rate of product release by

dx.doi.org/10.1021/bi3014104 | Biochemistry 2013, 52, 1755–1764

recording the fluorescence change upon rapid dilution of the enzyme−product complex (E·GS−DNB). The experimental traces were fit to a single exponential, yielding a rate of product release of ∼118 s^{-1} (Figure 7), which cannot be rate-limiting

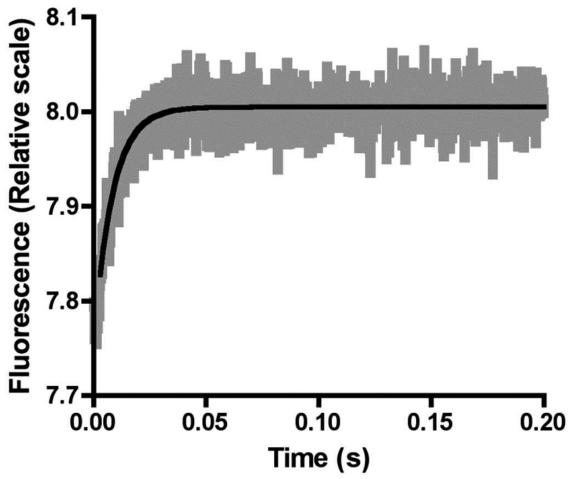

Figure 7. Product (GS−DNB) release was measured with stopped-flow protein fluorescence where MGST2 (40 μM), premixed with GSDNB (100 μM) in one syringe, was rapidly diluted with buffer in the other syringe. Final concentrations in the mixing chamber were 20 μM enzyme and 50 μM GSDNB. The experimental trace (gray) was fit to a single exponential (black line). A k of 118 s^{-1} was obtained by averaging three traces.

for the overall enzyme reaction (k_{cat} = 14.3 s^{-1}). An alternate attempt to confirm this conclusion by studying the viscosity dependence of k_{cat} could not be completed as the viscogens used (sucrose and glycerol) were inhibitory.

To summarize, we have given a full description of the kinetics and equilibrium of MGST2−GSH interaction, where a decrease in the pK_a of the thiol is an essential feature as expected. With regard to the overall catalysis, MGST2 activity is limited by the chemical conjugation step for second substrates that are less reactive than CDNB. With CDNB, the most reactive substrate used in this study, chemistry and thiolate anion formation rates begin to approach each other as evidenced by the burst kinetics of CDNB product formation (that becomes more pronounced at low GSH concentrations). The lack of saturation with CDNB in the burst kinetics precludes a direct measure of the chemical step. If K_D^{CDNB} is 1 mM, one can calculate from the value of k_4/K_D^{CDNB} that the chemical rate constant k_4 would be 10^2 s^{-1} and with a K_D^{CDNB} of 10 mM the rate constant would be 10^3 s^{-1}. The latter value compares with that for MGST1, taking into account the fact that experiments were performed at different temperatures.[19]

DISCUSSION

A common feature of GSH-activating enzymes is that they deprotonate glutathione to form the highly reactive GS^- at physiologic pH. This property has been described for other MAPEG enzymes such as LTC4S and MGST1. However, the substrate specificity, rate of GSH activation, and stoichiometry of binding differ between enzyme families and family members. Most GSTs are highly specific for GSH as a nucleophile but highly permissive with regard to the electrophilic second substrates.[16] Mechanistic studies of LTC4S have shown a different substrate profile with high specificity toward both the electrophilic LTA_4 and nucleophilic GSH where the activation of GSH, i.e., formation of thiolate anion (k_2), is very rapid in comparison to that of the related MGST1.[7,20] Furthermore, all the monomers of LTC4S are catalytically competent in forming a thiolate, in contrast to MGST1, which forms a thiolate in only one of three monomers;[21] it is therefore of interest to examine the behavior of MGST2, which is more closely related to LTC4S by sequence comparison but has broader substrate specificity putting it closer to MGST1.

The stoichiometry of MGST2 thiolate activation was analyzed by measuring the amplitude of the thiolate signal from determination of the rate of thiolate formation (Figure 4) as well as by measuring the amplitude of the catalytic burst from active site titrations (Figure 6A). The obtained signals suggest a thiolate:subunit protein stoichiometry of 1:3, similar to what has been seen for MGST1 but different from what has been observed for LTC4S. Furthermore, this suggested difference in thiolate:enzyme stoichiometry between MGST2 and LTC4S might be related to the respective physiological functions of these enzymes. Thus, LTC4S has evolved a high specificity toward the unstable LTA_4 with a need to be a rapid catalyst with all monomers able to form thiolate anions when the transient substrate LTA_4 is present. On the other hand, MGST2, which is more promiscuous with respect to substrates, displays characteristics similar to those of the detoxification enzyme MGST1 and has not evolved an efficiency similar to that of LTC4S in thiolate anion activation. However, further experiments need to be conducted to further ascertain that the observed thiolate subunit protein:MGST2 stoichiometry of 1:3 represents a mechanistic feature of MGST2 as we cannot at this point rule out the presence of the inactive enzyme in the preparation.

The observed rate of thiolate anion formation in MGST2 at 2 mM GSH was 18 s^{-1}, and the proton release experiment at the same concentration of GSH showed a rate of proton release of 9 s^{-1}. Thus, proton release could be an alternative to thiolate anion formation as limiting the rate of enzyme catalysis (when the chemical step is very rapid). As protonation and deprotonation are very rapid processes per se, we interpret the slow rate constants as signifying rate-limiting conformational transitions involved in GSH activation.

The binding affinity for the GSH thiolate was measured directly, $K_d^{GS^-}$ (136 ± 55 μM) (Figure 5). If we have an accurate model for GSH binding and deprotonation, the theoretical $K_d^{GS^-}$ value, calculated from the microscopic rate constants (k_2 = 41.1 s^{-1}, and k_{-2} = 2.0 s^{-1}) and the equilibrium constant (K_d^{GSH} = 4.3 mM) using eq VI, should be in reasonable agreement, which was indeed the case [compare the $K_d^{GS^-}$(calculated) value of 200 ± 70 μM with the $K_d^{GS^-}$(experimentally obtained) value of 136 ± 55 μM]. The k_{-2} obtained from the dilution experiment is used here because it gives a direct measurement of GS^- release.

$$K_d^{GS^-} = \frac{[E][GSH]}{[E{-}GSH]\left(1 + \frac{k_2}{k_{-2}}\right)} \quad \text{and} \quad K_d^{GSH} = \frac{[E][GSH]}{[E{-}GSH]}$$

$$\text{we get} \quad K_d^{GS^-} = \frac{K_d^{GSH}}{1 + \frac{k_2}{k_{-2}}} \qquad \text{(VI)}$$

Tables 1 and 3 show that MGST2 is a peroxidase displaying a K_M in the range of 5−20 μM, comparable with that observed

dx.doi.org/10.1021/bi3014104 | Biochemistry 2013, 52, 1755−1764

for GSH-dependent peroxide reducing enzymes like hGSTA1-1 (K_M of 5 μM). Peroxidase activities play an important role in the regulation of the biosynthesis of the pro-inflammatory leukotrienes and prostaglandins via 5-lipoxygenase and cyclooxygenase enzymes,[22] and both these oxygenases require a saturating "peroxide tone" (concentration of hydroperoxides)[23] for catalysis. The observed efficient peroxidase activity of MGST2 suggests that it may be indirectly involved in regulating arachidonic acid metabolism and formation of lipid mediators as has been shown for certain Se-dependent GSH peroxidases.[24]

LTC_4 production by membrane preparations of MGST2 has been described previously,[11,25] but here, for the first time, purified MGST2 is analyzed allowing for direct comparisons of k_{cat}/K_M values. MGST2 displays a 48 times lower efficiency in LTC_4 production than LTC4S.

Upon comparison of relative specific activities (Table 2), rather than catalytic parameters, of MGST2 (1.2 μmol min^{-1} mg^{-1}), LTC4S (35 μmol min^{-1} mg^{-1}),[7] cytosolic GSTs (2−10 nmol min^{-1} mg^{-1}),[26] and MGST1 (0.2 nmol min^{-1} mg^{-1}), the latter two display a substantially lower activity toward LTA_4 as the electrophilic substrate,[25] suggesting that MGST2 could play a physiological role in LTC_4 formation, as has been previously proposed on the basis of experiments both in vitro and in vivo.[9,10,12]

A striking difference between LTC4S and MGST2 is the ability to conjugate GSH with CDNB (Tables 1 and 3). CDNB is an artificial substrate often used to study catalytic mechanisms of xenobiotic metabolizing GSTs. To obtain a complete description of the kinetic mechanism, we decided to use CDNB and its product to analyze the rate-limiting step(s) of MGST2.

First, product release (of the CDNB−GSH conjugate, 118 s^{-1}) is not rate-limiting (Figure 7) for k_{cat} (14.3 s^{-1}). Bursts of product formation with CDNB set a lower limit for the rate constant of the chemical step (our estimate of k_4 of $\geq 10^2$ s^{-1}). The chemical step for CDNB is thus comparable to or higher than that for thiolate anion formation (k_2 = 41 ± 1.2 s^{-1}). Clearly for all other less reactive substrates, chemistry will determine k_{cat} (e.g., Table 3). However, in normal physiology, reactive electrophiles will be present in small amounts, and k_{cat}/K_M will determine the reaction rate. Judging from the Hammett plot (Figure 2) the more reactive the substrate becomes, the faster it will be eliminated in direct proportion to reactivity, which appears to be an efficient strategy for xenobiotic metabolism also seen with other GSTs.[15,27]

In summary, MGST2 displays a wide substrate specificity, including LTA_4 and lipid peroxides. MGST2 is relatively efficient in conjugating LTA_4 with GSH, suggesting a physiologic role of MGST2 as a pro-inflammatory biosynthetic enzyme. The mechanistic study suggests the third-of-the-sites reactivity also seen for the related MGST1 (but in contrast to what has been found for LTC4S), with the chemical step being rate-limiting under physiological conditions.

AUTHOR INFORMATION

Corresponding Author

*E-mail: agnes.rinaldo-matthis@ki.se. Phone: +46-8-52487648. Fax: +46-8-7360439.

Funding

This work was supported by grants from the Swedish Research Council (to A.R.-M., J.Z.H., and R.M.).

Notes

The authors declare no competing financial interest.

ACKNOWLEDGMENTS

We gratefully thank Eva Ohlson and Michaela Mårback for technical assistance. We also thank Cristoph von Ballmos (Stockholm University, Stockholm, Sweden) for the help with the stopped-flow apparatus.

ABBREVIATIONS

cys-LTs, cysteinyl-leukotrienes; CDNB, 1-chloro-2,4-dinitrobenzene; CNBAL, 4-chloro-3-nitrobenzaldehyde; CNBAM, 4-chloro-3-nitrobenzamide; CNAP, 4-chloro-3-nitrobenzacetophenone; 4-HNE, 4-hydroxynonenal; DDM, dodecyl maltoside; GSH, glutathione; LT, leukotriene; 5-LO, 5-lipoxygenase; LTA_4, 5(*S*)-*trans*-5,6-oxido-7,9-*trans*-11,14-*cis*-eicosatetraenoic acid; LTC_4, 5(*S*)-hydroxy-6(*R*)-*S*-glutathionyl-7,9-*trans*-11,14-*cis*-eicosatetraenoic acid; LTD_4, 5(*S*)-hydroxy-6(*R*)-*S*-cysteinyl-glycyl-7,9-*trans*-11,14-*cis*-eicosatetraenoic acid; LTE_4, 5(*S*)-hydroxy-6(*R*)-*S*-cysteinyl-7,9-*trans*-11,14-*cis*-eicosatetraenoic acid; 5-HpETE, 5-hydroperoxyeicosatetraenoic acid; 15-HpETE, 15-hydroperoxyeicosatetraenoic acid; 13-HpODE, 13-hydroperoxyoctadecatetraenoic acid; 13-HpOTrE, 13-hydroperoxyoctadecatrienoic acid; hLTC4S, human leukotriene C_4 synthase; MGST, microsomal GSH transferase; MAPEG, membrane-associated proteins in eicosanoid and glutathione metabolism; mPGES1, microsomal PGE synthase; GSO_3^-, glutathione sulfonic acid, (2*S*)-2-amino-5-{[(2*R*)-1-(carboxymethylamino)-1-oxo-3-sulfopropan-2-yl]amino}-5-oxopentanoic acid.

REFERENCES

(1) Bresell, A., Weinander, R., Lundqvist, G., Raza, H., Shimoji, M., Sun, T. H., Balk, L., Wiklund, R., Eriksson, J., Jansson, C., Persson, B., Jakobsson, P. J., and Morgenstern, R. (2005) Bioinformatic and enzymatic characterization of the MAPEG superfamily. *FEBS J. 272*, 1688−1703.

(2) Jakobsson, P. J., Morgenstern, R., Mancini, J., Ford-Hutchinson, A., and Persson, B. (1999) Common structural features of MAPEG: A widespread superfamily of membrane associated proteins with highly divergent functions in eicosanoid and glutathione metabolism. *Protein Sci. 8*, 689−692.

(3) Martinez Molina, D., Eshaghi, S., and Nordlund, P. (2008) Catalysis within the lipid bilayer-structure and mechanism of the MAPEG family of integral membrane proteins. *Curr. Opin. Struct. Biol. 18*, 442−449.

(4) Haeggstrom, J. Z., Rinaldo-Matthis, A., Wheelock, C. E., and Wetterholm, A. (2010) Advances in eicosanoid research, novel therapeutic implications. *Biochem. Biophys. Res. Commun. 396*, 135−139.

(5) Martinez Molina, D., Wetterholm, A., Kohl, A., McCarthy, A. A., Niegowski, D., Ohlson, E., Hammarberg, T., Eshaghi, S., Haeggström, J. Z., and Nordlund, P. (2007) Structural basis for synthesis of inflammatory mediators by human leukotriene C4 synthase. *Nature 448*, 613−616.

(6) Rinaldo-Matthis, A., Wetterholm, A., Molina, D. M., Holm, J., Niegowski, D., Ohlson, E., Nordlund, P., Morgenstern, R., and Haeggstrom, J. Z. (2010) Arginine 104 is a key catalytic residue in leukotriene C4 synthase. *J. Biol. Chem. 285*, 40771−40776.

(7) Rinaldo-Matthis, A., Ahmad, S., Wetterholm, A., Lachmann, P., Morgenstern, R., and Haeggstrom, J. Z. (2012) Pre-steady-state kinetic characterization of thiolate anion formation in human leukotriene C synthase. *Biochemistry 51*, 848−856.

(8) Saino, H., Ukita, Y., Ago, H., Irikura, D., Nisawa, A., Ueno, G., Yamamoto, M., Kanaoka, Y., Lam, B. K., Austen, K. F., and Miyano, M.

(2011) The catalytic architecture of leukotriene C4 synthase with two arginine residues. *J. Biol. Chem. 286*, 16392−16401.
(9) Kanaoka, Y., Maekawa, A., Penrose, J. F., Austen, K. F., and Lam, B. K. (2001) Attenuated zymosan-induced peritoneal vascular permeability and IgE-dependent passive cutaneous anaphylaxis in mice lacking leukotriene C4 synthase. *J. Biol. Chem. 276*, 22608−22613.
(10) Scoggan, K. A., Jakobsson, P. J., and Ford-Hutchinson, A. W. (1997) Production of leukotriene C4 in different human tissues is attributable to distinct membrane bound biosynthetic enzymes. *J. Biol. Chem. 272*, 10182−10187.
(11) Jakobsson, P. J., Mancini, J. A., and Ford-Hutchinson, A. W. (1996) Identification and characterization of a novel human microsomal glutathione S-transferase with leukotriene C4 synthase activity and significant sequence identity to 5-lipoxygenase-activating protein and leukotriene C4 synthase. *J. Biol. Chem. 271*, 22203−22210.
(12) Sjostrom, M., Jakobsson, P. J., Heimburger, M., Palmblad, J., and Haeggstrom, J. Z. (2001) Human umbilical vein endothelial cells generate leukotriene C4 via microsomal glutathione S-transferase type 2 and express the CysLT(1) receptor. *Eur. J. Biochem. 268*, 2578−2586.
(13) Lowry, O. H., Rosebrough, N. J., Farr, A. L., and Randall, R. J. (1951) Protein measurement with the Folin phenol reagent. *J. Biol. Chem. 193*, 265−275.
(14) Bradford, M. M. (1976) A rapid and sensitive method for the quantitation of microgram quantities of protein utilizing the principle of protein-dye binding. *Anal. Biochem. 72*, 248−254.
(15) Morgenstern, R., Lundqvist, G., Hancock, V., and DePierre, J. W. (1988) Studies on the activity and activation of rat liver microsomal glutathione transferase, in particular with a substrate analogue series. *J. Biol. Chem. 263*, 6671−6675.
(16) Mosialou, E., Piemonte, F., Andersson, C., Vos, R. M., van Bladeren, P. J., and Morgenstern, R. (1995) Microsomal glutathione transferase: Lipid-derived substrates and lipid dependence. *Arch. Biochem. Biophys. 320*, 210−216.
(17) Graminski, G. F., Kubo, Y., and Armstrong, R. N. (1989) Spectroscopic and kinetic evidence for the thiolate anion of glutathione at the active site of glutathione S-transferase. *Biochemistry 28*, 3562−3568.
(18) Caccuri, A. M., Lo Bello, M., Nuccetelli, M., Nicotra, M., Rossi, P., Antonini, G., Federici, G., and Ricci, G. (1998) Proton release upon glutathione binding to glutathione transferase P1-1: Kinetic analysis of a multistep glutathione binding process. *Biochemistry 37*, 3028−3034.
(19) Svensson, R., Alander, J., Armstrong, R. N., and Morgenstern, R. (2004) Kinetic characterization of thiolate anion formation and chemical catalysis of activated microsomal glutathione transferase 1. *Biochemistry 43*, 8869−8877.
(20) Morgenstern, R., Svensson, R., Bernat, B. A., and Armstrong, R. N. (2001) Kinetic analysis of the slow ionization of glutathione by microsomal glutathione transferase MGST1. *Biochemistry 40*, 3378−3384.
(21) Alander, J., Lengqvist, J., Holm, P. J., Svensson, R., Gerbaux, P., Heuvel, R. H., Hebert, H., Griffiths, W. J., Armstrong, R. N., and Morgenstern, R. (2009) Microsomal glutathione transferase 1 exhibits one-third-of-the-sites-reactivity towards glutathione. *Arch. Biochem. Biophys. 487*, 42−48.
(22) Rinaldo-Matthis, A., and Haeggstrom, J. Z. (2010) Structures and mechanisms of enzymes in the leukotriene cascade. *Biochimie 92*, 676−681.
(23) Smith, W. L. (2005) Cyclooxygenases, peroxide tone and the allure of fish oil. *Curr. Opin. Cell Biol. 17*, 174−182.
(24) Flohe, L. (2010) Changing paradigms in thiology from antioxidant defense toward redox regulation. *Methods Enzymol. 473*, 1−39.
(25) Schroder, O., Sjostrom, M., Qiu, H., Stein, J., Jakobsson, P. J., and Haeggstrom, J. Z. (2003) Molecular and catalytic properties of three rat leukotriene C_4 synthase homologs. *Biochem. Biophys. Res. Commun. 312*, 271−276.
(26) Soderstrom, M., Hammarstrom, S., and Mannervik, B. (1988) Leukotriene C synthase in mouse mastocytoma cells. An enzyme distinct from cytosolic and microsomal glutathione transferases. *Biochem. J. 250*, 713−718.
(27) Chen, W. J., Graminski, G. F., and Armstrong, R. N. (1988) Dissection of the catalytic mechanism of isozyme 4-4 of glutathione S-transferase with alternative substrates. *Biochemistry 27*, 647−654.